Chemistry–A European Journal
Research Article
doi.org/10.1002/chem.202302347
Chemistry Europe
European Chemical Societies Publishing
www.chemeurj.org

Hot Paper

Reductive Activation of Aryl Chlorides by Tuning the Radical Cation Properties of *N*-Phenylphenothiazines as Organophotoredox Catalysts

Fabian Weick,[a] Nina Hagmeyer,[b] Madeleine Giraud,[a] Benjamin Dietzek-Ivanšić,*[b, c] and Hans-Achim Wagenknecht*[a]

Aryl chlorides as substrates for arylations present a particular challenge for photoredox catalytic activation due to their strong C(sp^2)–Cl bond and their strong reduction potential. Electron-rich *N*-phenylphenothiazines, as organophotoredox catalysts, are capable of cleaving aryl chlorides simply by photoinduced electron transfer without the need for an additional electrochemical activation setup or any other advanced photocatalysis technique. Due to the extremely strong reduction potential in the excited state of the *N*-phenylphenothiazines the substrate scope is high and includes aryl chlorides both with electron-withdrawing and electron-donating substituents. We evidence this reactivity for photocatalytic borylations and phosphonylations. Advanced time-resolved transient absorption spectroscopy in combination with electrochemistry was the key to elucidating and comparing the unusual photophysical properties not only of the *N*-phenylphenothiazines, but also of their cation radicals as the central intermediates in the photocatalytic cycle. The revealed photophysics allowed the excited-state and radical-cation properties to be fine-tuned by the molecular design of the *N*-phenylphenothiazines; this improved the photocatalytic activity.

Introduction

The synthetic route to arylated organic compounds is one of the most important tasks in organic synthesis for all kinds of disciplines, such as pharmaceutical, medicinal, dye and material chemistry. Thus, arylations are also a research focus of photoredox catalysis[1] to enhance the sustainability by using light as energy source and metal-free catalysts.[2] Early examples of arylations were achieved by using aryl diazonium salts,[3] diaryliodonium salts,[4] triphenylsulfonium salts,[5] sulfonyl chlorides,[6] acyl hypobromites[7] and Katritzky salts[8] as reactive precursors (Figure 1). These compounds (ArX) were activated by reduction through a single electron transfer from the photoredox catalyst in the excited state, which induces cleavage of the leaving group and yields highly reactive aryl radicals. The reduction potentials are in the range between $E_{red}(ArX/ArX^{\bullet-}) = -0.1$ V (vs. SCE) for the diazonium salts and $E_{red}(ArX/ArX^{\bullet-}) = -1.5$ V for the triphenylsulfonium salts. Accordingly, these aryl radical precursors can be activated by conventional transition metal photoredox catalysts, mainly $[Ru(bpy)_3]^{2+}$ and $Ir(ppy)_3$. However, the use of the mentioned synthetic precursors requires additional efforts because they are not stable and must be freshly prepared prior to the arylations. Aryl halides, on the other hand, are commercially available in great variety, are bench stable and exhibit enormous diversity in their substitution pattern. Aryl iodides (ArI) with a reduction potential of $E_{red}(ArI/ArI^{\bullet-}) = -2.0$ V and bromides (ArBr), $E_{red}(ArBr/ArBr^{\bullet-}) = -2.4$ V, have successfully been activated and used as precursors for arylations using organophotoredox catalysts, for example, rhodamine 6G. Aryl chlorides (ArCl) present a particular challenge for photoredox catalytic activation due to the strong C(sp^2)–Cl bond of 97 kcal mol^{-1} (in chlorobenzene) and the strong reduction potential of $E_{red}(ArCl/ArCl^{\bullet-}) = -2.8$ V. Advanced photoredox catalytic concepts are needed to overcome these problems. König et al. used aryl chlorides with electron-withdrawing substituents for arylations by the consecutive photoelectron transfer concept (conPET) with perylene bisimides as photocatalysts.[9] This was further developed to the sensitization-initiated electron transfer (SenI-ET) for photoredox catalytic activation of aryl chlorides, but is still limited to those with electron-withdrawing groups and *N*-heterocycles.[10] The conPET concept was also applied to cyanoarenes as organophotocatalysts by Wu et al. to obtain extreme photoreduction potentials

[a] Dr. F. Weick, M. Giraud, Prof. Dr. H.-A. Wagenknecht
Institute of Organic Chemistry
Karlsruhe Institute of Technology (KIT)
Fritz-Haber-Weg 6, 76131 Karlsruhe (Germany)
E-mail: Wagenknecht@kit.edu
Homepage: www.ioc.kit.edu/wagenknecht/

[b] N. Hagmeyer, Prof. Dr. B. Dietzek-Ivanšić
Institute of Physical Chemistry
Friedrich Schiller University Jena
Lessingstraße 4, 07743 Jena (Germany)
E-mail: benjamin.dietzek@uni-jena.de
Homepage: www.ipc.uni-jena.de/en/agdietzek

[c] Prof. Dr. B. Dietzek-Ivanšić
Research Department Functional Interfaces
Leibniz Institute of Photonic Technology Jena
Albert-Einstein-Straße 9, 07745 Jena (Germany)

Supporting information for this article is available on the WWW under https://doi.org/10.1002/chem.202302347

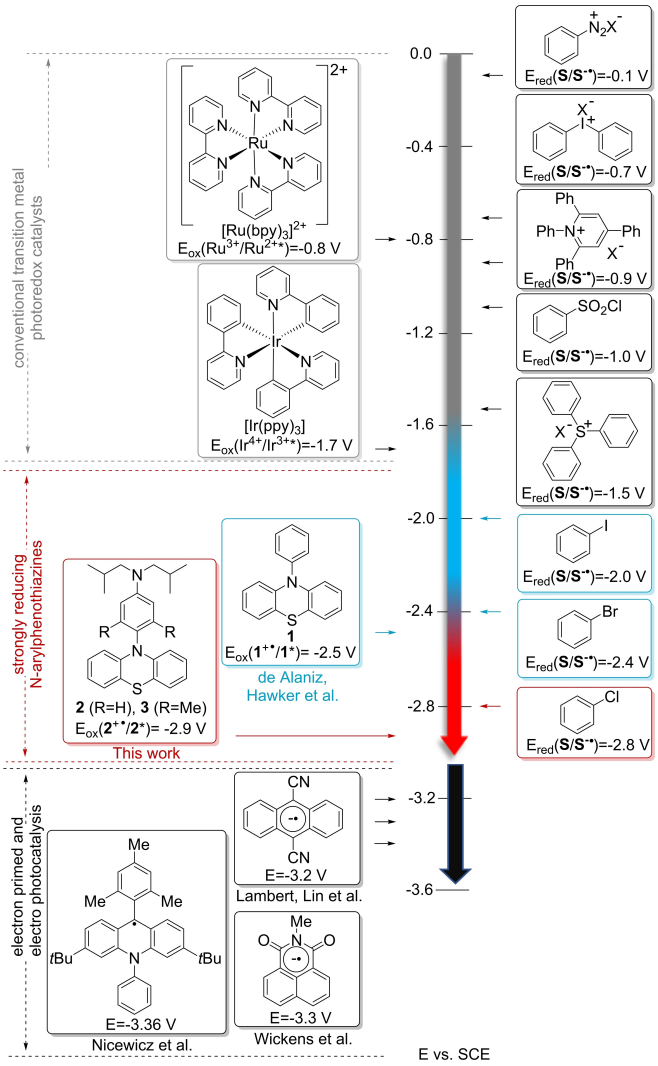

Figure 1. Redox potentials of *N*-phenylphenothiazines **1**–**3** as strongly reducing organo-photocatalysts in comparison to conventional transition metal photocatalysts, electron-primed and electrochemical photocatalysis and substrates (**S**) for aryl radical formation by single electron transfer. Top: Previous photocatalytic approaches to activate aryl chlorides from the literature.

and to access aryl radicals from aryl chlorides.[11] Using the conPET process Nicewicz et al. were able to use the acridine radical with an excited state potential of −3.36 V for dehalogenation of aryl chlorides, but this requires $(i\text{Pr})_2$NEt as additive and sacrificial electron donor that undergoes conversion to its radical with an unclear fate.[12] Electron-primed photoredox catalysis (epPRC) replaces the need for such an additive by the use of electrochemistry and is also able to unlock aryl chlorides as shown by Wickens et al.[13] The photoelectrochemical strategy[14] was then further developed to reductive electrophotocatalysis by Lambert, Lin et al.; they achieved excited radical anions of dicyanoanthracene with a reduction potential of −3.2 V.[15] However, electro-photocatalysis requires an electrochemical setup in addition to the conventional and in most cases rather simple irradiation setup. Based on the aforementioned reduction potential, electro-photocatalysis should not be required for the photocatalytic conversion of aryl chlorides.

Hawker, de Alaniz et al. transferred *N*-phenylphenothiazine (Ppt) from atom radical transfer polymerization (ATRP)[16] to photoredox catalysis[17] and achieved dehalogenation of aryl chlorides. They assumed a one-photon process, although the excited state potential of this photocatalyst, $E_{ox}(\text{Ppt}^{\bullet+}/\text{Ppt}^*) = -2.5$ V, is not sufficiently high to photoreduce aryl chlorides. The use of *N*-phenylphenothiazines for activation of aryl precursors was further developed by Larionov et al. and applied also for the borylation of some aryl chlorides.[18] Meyer and Hu unraveled the two-photon activation of *N*-phenylphenothiazine, determined $E_{red}(\text{Ppt}^{\bullet+}*/\text{Ppt}) = 2.3$ V which was sufficient to oxidize chloride.[19] *N*,*N*-Diarylphenazines are not more strongly reducing photocatalysts than *N*-phenylphenothiazines.[20] However, arylamines are in general more strongly reducing chromophores.[21] Accordingly, we further developed the phenyl module of phenothiazines by different types of substituents to reach stronger reduction potentials.[22] We present herein three electron-rich phenothiazines **1**–**3** capable of activating aryl chlorides simply by reduction via photoredox catalysis without the need for an additional electrochemical activation setup or any other advanced photocatalysis technique. We apply advanced time-resolved transient absorption spectroscopy in combination with electrochemistry to unravel the unusual photophysical properties of **1**–**3**, but also of the cation radicals $\mathbf{1}^{\bullet+}$–$\mathbf{3}^{\bullet+}$ as key intermediates in the photocatalytic cycle. These excited-state processes and photophysics are of utmost importance to gain valuable mechanistic insights and to improve the photocatalytic activity. This tuning of the radical cation properties yielded a broad substrate scope including both aryl chlorides with electron-withdrawing and electron-donating substituents. We evidence this reactivity for photocatalytic borylations and phosphonylations.

Results and Discussion

N-Phenylphenothiazines as strongly reducing organophotoredox catalysts

The tunability of organophotoredox catalysts is a prerequisite to adjust their applicability to distinct organic reactions.[23] *N*-phenylphenothiazines[19,22–24] based on the core structure **1** fulfill this requirement in principle through their modular structure, as they can be modified at the core or at the phenyl substituents to vary the optoelectronic properties and adapt the photoredox properties to the particular synthetic problem. The introduction of dialkylamino substituents in the para position on the phenyl ring give strongly negative redox potentials.[23a] The catalyst *N*-(4-*N*,*N*-diisobutylaminophenyl)phenothiazine (**2**) is characterized by an excited state reduction potential of $E_{ox}(\mathbf{2}^{\bullet+}/\mathbf{2}^*) = -2.9$ V in the singlet (S_1) state (Figure 2).[22] This allowed us to activate not only styrene derivatives,[23a] such as α-methylstyrene ($E_{red} = -2.5$ to −2.7 V), but also aliphatic olefins ($E_{red} = -3.0$ V).[25] In addition, a novel phenothiazine, *N*-(4-*N*,*N*-diisobutylamino-2,5-

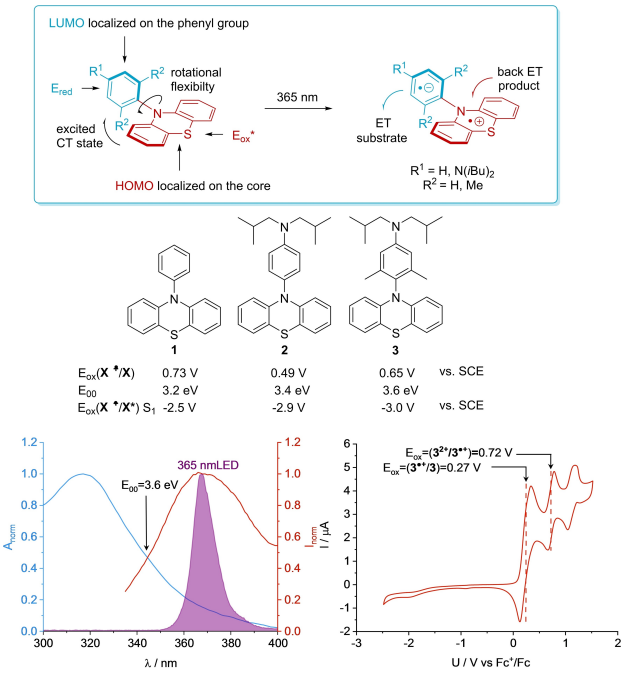

Figure 2. Photochemistry of *N*-phenylphenothiazines **1**–**3** with the expected charge-separated state for photoredox catalysis (top), structures and electrochemical properties (middle), and absorbance, fluorescence (including the normalized emission of the 365 nm LED) and cyclic voltammetry (100 mV s^{-1} in MeCN) of **3** (bottom vs. Fc^+/Fc as standard; the two potentials were converted to SCE by $\Delta E = +0.38$ V: 1) $E_{ox}(\mathbf{3}^{\bullet+}/\mathbf{3}) = 0.65$ V and 2) $E_{ox}(\mathbf{3}^{2+}/\mathbf{3}^{\bullet+}) = 1.10$ V).

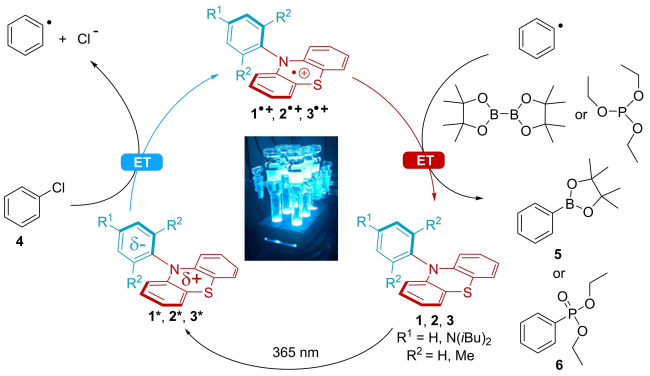

Figure 3. The basic photoredox catalytic cycle includes the absorption of one photon for activation of the substrate chlorobenzene (**4**) to the phenyl radical and subsequent formation of the borylated product **5** and the phosphonylated product **6**, respectively.

dimethylphenyl)phenothiazine (**3**) was synthesized bearing two additional methyl groups in *ortho*-position of the coupled aromatic system to increase the rotational barrier. This structural change was expected to affect the catalytic activity by a longer-lived charge-separated state, similar to mesitylacridinium as photocatalyst.[26] Cyclic voltammetry of **3** revealed a redox potential of $E_{ox}(\mathbf{3}^{\bullet+}/\mathbf{3}) = 0.65$ V. Together with $E_{00} = 3.6$ eV for the S_1 state, the excited state redox potential was estimated to be $E_{ox}(\mathbf{3}^{\bullet+}/\mathbf{3}^*) = -3.0$ V. Obviously, the +I effect of the additional methyl groups shifts the potential by approximately 0.1 V compared to **2**. It is important to mention that the 365 nm LED is not monochromatic and has a rather broad emission that includes the wavelength equivalent to $E_{00} = 3.6$ eV (345 nm).

Photoredox catalytic activation of aryl chlorides and reaction scope

After photoreduction of aryl chlorides and homolytic bond cleavage of the C(sp^2)–Cl bond, a highly reactive aryl radical is formed. This can be used for various synthetic purposes depending on how it is captured by the chosen reaction partners. In this work, two different reaction types were selected and investigated (Figure 3). First, photoredox catalytic borylations were considered, as bis(pinacolato)diborone can rapidly scavenge aryl radicals, subsequently forming aryl boronic esters. Thus, this reaction is well suited to demonstrate photoredox catalytic activation of the aryl chloride. In addition, borylation reactions are also of great importance synthetically, as they provide access to aryl boronic acid esters, which are important building blocks for Suzuki-Miyaura couplings.[27] To be able to optimize the reaction conditions, chlorobenzene (**4**) was used as simple substrate at the beginning. It is converted to phenylboronic acid pinacol ester (**5**) with bis(pinacolato)diborane in the presence of the phenothiazines **1**–**3** upon irradiation with a 365 nm LED. Under standard conditions (Table 1), the yield could be increased from 43 to 87% when photocatalyst **2** was used instead of the reference photocatalyst **1**. Photocatalyst **3** decreased the yield to 57%. This was an unexpected result because we assumed that the decreased rotational flexibility by the two *ortho*-methyl groups would extend the charge-separated state lifetime and thereby improve the photocatalytic potency of **3**. The photoredox catalytically generated aryl radicals can alternatively be scavenged by trivalent phosphites to form phosphonates. These phosphorylations complement Arbusov reactions[28] which are

Table 1. Screening of the yields for the conversion of chlorobenzene (**4**) as substrate into the borylated product **5** and the phosphonylated product **6**.

	Photocatalyst[a]	Yield [%]	
		5[b,d]	**6**[c,d]
1	**1**	43	55
2	**2**	87	67
3	**3**	57	48
4	–	20	1
5	**2**, no $NaCHO_2$	54	22
6	**2**, no Cs_2CO_3	0	0
7	**2**, no light	1	0
8	**1**, $(i\text{Pr})_2\text{NEt}$[e]	32	41

[a] 0.2 mM **4** in 1 mL total volume (0.2 M), 10 mol% **1**–**3**, MeCN. [b] 3.0 equiv. bis(pinacolato)diborone, 3.0 equiv. Cs_2CO_3, 3.0 equiv. $NaCHO_2$, 24 h, 365 nm LED. [c] 3.0 equiv. triethylphosphites, 3.0 equiv. Cs_2CO_3, 3.0 equiv. $NaCHO_2$, 65 h, 365 nm LED. [d] All photocatalytic experiments were done as triplicates and average yields were reported. [e] Instead of Cs_2CO_3.

reactions of trialkyl phosphites with alkyl halides in an S_N2 mechanism. The products are important building blocks for the Horner-Wadsworth-Emmons olefinations.[29] Aryl phosphonates are also of particular synthetic interest as precursors for next-generation phosphine ligands.[30] The conventional Arbusov reaction cannot be used for the synthesis of arylphosphonates. Hence, our photocatalytic version is not only an alternative to the Arbusov reaction but complements the conventional reaction. Analogous to the borylation reaction already discussed above, a phenyl radical is also formed here after reduction of the chlorobenzene (**4**) by the photoredox catalyst **2** upon irradiation at 365 nm, but then captured by the triethyl phosphite. With the additive sodium formate as H-atom transfer (HAT) reagent product **6** is formed. The dependence of the yields on the different photocatalyst is not as strong as for the borylation described above, but is still observable. Using photocatalyst **1**, product **6** is formed in 55% yield, photocatalyst **2** slightly increases the yield to 67%, and photocatalyst **3** decreases the yield to 48%. Control reactions without any photocatalyst, without Cs_2CO_3 as base and without light gave product **6** only in traces, if at all. The base is essential for both photocatalytic reactivities. For the borylations, the base activates the bis(pinacolato)diborane. In the case of the phosphonylations, the role of the base is not the sacrificial electron donor; it is more likely that it promotes the cleavage of the phosphone intermediate after attack of the phenyl radical. Cs_2CO_3 might be replaced by $(i\text{Pr})_2\text{NEt}$ as organic base, but the yields drop to approximately 75% compared to the yields achieved with Cs_2CO_3. The HAT reagent $NaHCO_2$ only improves the yield, but is not crucial, since product **5** is obtained in 54% yield and product **6** in 22% yield without this additive. This supports the mechanism that the HAT reagent promotes the back electron transfer which is coupled to a proton transfer.

Mechanistic studies by means of time-resolved spectroscopy

It was demonstrated above that, despite their structural similarities, the catalysts presented in this work yield different photocatalytic efficiencies. We performed femtosecond transient absorption (fs-TA) and transient absorption spectro-electrochemistry (TA-SEC) under oxidative conditions to characterize the photocatalysts' excited-state behavior and to identify photophysical properties trying to rationalize the different photocatalytic performances. Figure 4 shows the transient absorption spectra of **2** in acetonitrile (MeCN) upon excitation at 330 nm. For quantitative analysis, a multiexponential global fit was applied. The resulting decay-associated spectra (DAS) are shown in Figures S19–S21 in the Supporting Information. At early delay times, the compound shows excited-state absorption (ESA) bands with maxima at 375 and 640 nm. Based on literature, these spectral features are attributed to the excited singlet state of the phenothiazine.[31] Both bands decay on a nanosecond timescale while a new absorption band at 450 nm arises simultaneously. The observed changes are assigned to intersystem crossing (ISC) forming a triplet state[31,32] which has a lifetime beyond the 2 ns delay time range accessible by the femtosecond-transient absorption setup. Kinetic analysis reveals the presence of an additional, comparably fast process characterized by a characteristic time constant of ~10 ps. Following the argument made by Wasielewski et al.[33] for compound **1** (Figure S20), we assign this fast process to intramolecular torsional relaxation in the excited state.

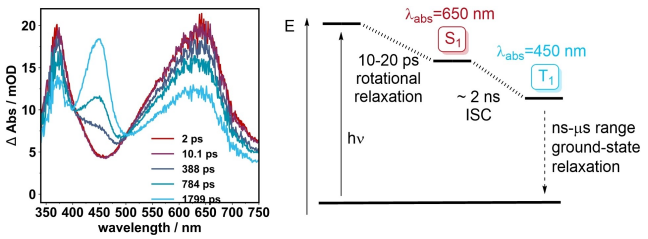

Figure 4. Transient absorption spectra of **2** in acetonitrile after excitation at 330 nm at different delay times and simplified Jablonski diagram of **2**.

The transient absorption spectra of compounds **1** and **3** (Figures S20 and S21) do not reveal marked differences compared to **2**, neither in regard to spectral features nor in the kinetic constants obtained. Therefore, these data describing the photochemical properties of the photocatalysts **1**–**3** do not account for the observed catalytic differences. A detailed examination of the long-lived (triplet) state of the phenothiazines beyond an estimate of their singlet excited state redox potentials (Figure 1) was not performed. To estimate the possible involvement of triplet states in the catalytic cycle, we referred to triplet state energies of related phenothiazines.[34] The literature, which is, for example, based on phosphorescence measurements, reports triplet state energies at around 2.6 eV. Assuming similar energies for the phenothiazines investigated in this work, the triplet state is not expected to reductively activate chlorobenzene as the resulting excited state reduction potentials are not sufficiently negative.

This led us to investigate the photophysical behavior of the corresponding cation radicals by steady-state and time-resolved spectro-electrochemical methods. As the radical species $\mathbf{1}^{\bullet+}$–$\mathbf{3}^{\bullet+}$ of the catalysts are formed upon the first light-induced electron transfer and are postulated to participate in the back electron transfer during the catalytic cycle, we assumed that the tuning of the radical cation accounts for the photocatalytic activity. Therefore, the investigation of their photophysical properties is expected to give valuable mechanistic insight.

It is known from literature that oxidation of **1** yields the red radical cation $\mathbf{1}^{\bullet+}$ with absorption peaks at 515, 700, 770 and 865 nm (Figure 5).[33,35] With that it closely resembles the absorption spectrum of the radical cation of N-alkyl-substituted phenothiazines which do not bear an aromatic substituent in the 10-position.[36] This indicates that the phenyl substituent does not contribute to the absorption in the visible range meaning that the optical transitions are limited to the phenothiazine core where the radical cation is localized. The same applies for $\mathbf{3}^{\bullet+}$ which shows identical spectral features (Figure S22). Oxidation of **2**, however, results in a blue solution with a significantly different absorption spectrum (Figures 5 and S23). This indicates that there is an interaction between the phenothiazine core and the aromatic substituent allowing the

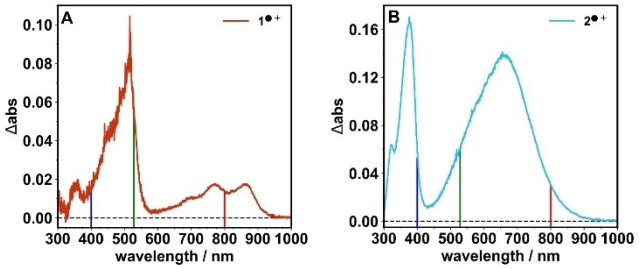

Figure 5. UV/Vis difference absorption spectra of the electrochemically generated radical cations of A) **1** and B) **2** in MeCN containing 0.1 M $TBAPF_6$ (scan rate 100 mV s^{-1}, glassy carbon working electrode, Pt counter electrode and Ag/AgCl pseudo-reference electrode).

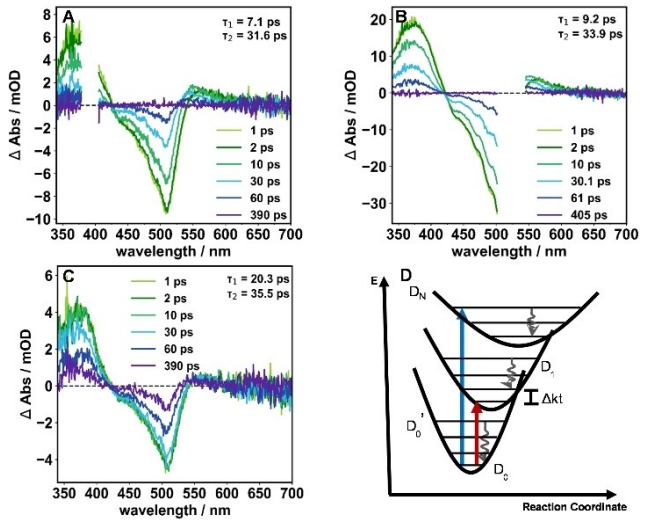

Figure 6. Transient absorption spectra at selected delay times for electrochemically generated $\mathbf{1}^{\bullet+}$ in MeCN pumped at A) 400, B) 528 and C) 800 nm. D) The proposed relaxation pathway. For the DAS, see Figure S24.

π-system to delocalize over both parts of the molecular structure. Similar results are reported for 10-(4-dimethylaminophenyl)phenothiazine for which EPR measurements suggest a Wurster's blue type radical which is no longer phenothiazine-based but localized on the aromatic π-system of the substituent as well as both nitrogen atoms.[37] However, comparison of the absorption spectra of Wurster's blue and $\mathbf{2}^{\bullet+}$ reveals distinct differences indicating that, in $\mathbf{2}^{\bullet+}$, the chromophore comprises both units, the phenothiazine and the N-bisalkylated phenyl ring. Based on the shape of the spectra we hypothesize that the electron-donating character of the additional alkylamino group results in a hypsochromic shift of the absorption bands. As a result, the bands at 515 and 600 to 900 nm of $\mathbf{1}^{\bullet+}$ are shifted to 375 and 450 to 900 nm. The absence of this effect in $\mathbf{3}^{\bullet+}$, despite the presence of the alkylamino substituent, is most likely due to steric hindrance because of the additional methyl groups. These are expected to hamper rotation of the aromatic ring and inhibit the system to adapt a molecular geometry in which efficient electronic coupling between the phenothiazine core and the aromatic ring is possible which would result in the blue-shifted absorption band of the radical. These steady-state absorption spectra already imply that the radicals might show distinctly different excited-state behavior which was studied in the next step.

Transient absorption spectra of the chemically generated cation radical $\mathbf{1}^{\bullet+}$ have already been reported by Wasielewski et al.[35] Here, we employed TA-SEC using excitation wavelengths of 400, 530 and 800 nm to investigate the excited-state processes of $\mathbf{1}^{\bullet+}$ (Figure 6). The resultant data agree well with the ones reported for chemical oxidation.[35] The spectra show ESA with maxima at 370 and 560 nm and a ground-state bleach (GSB) between 430 to 540 nm. Relaxation to the ground state takes place on a sub-nanosecond timescale. The data were best fitted with a sum of two exponentials resulting in time constants of 7.1 and 9.2 ps as well as 31.6 and 33.9 ps for pump wavelengths of 400 and 528 nm, respectively. For excitation at 800 nm the first characteristic delay time becomes longer, more specifically 20.3 ps, which is similar to what has been observed by others,[35] who interpreted these kinetic processes as a relaxation within the D_1 (doublet) excited state, which then relaxes back to the electronic ground state, D_0.[35] This relaxation scheme does, however, not capture the prolongation of the first characteristic time constant upon shifting the excitation wavelength to 800 nm in a straight-forward manner. Therefore, we propose a slightly modified model (Figure 6 D), which ascribes τ_1 to a transition from the electronically excited state D_1 to a hot ground state D_0'. Subsequently, relaxation to the thermally equilibrated ground state D_0 takes place on a 30-ps timescale. This timescale is consistent with reports on ground-state relaxation dynamics as, for example, reported for 4-di(4′-*tert*-butylbiphenyl-4-yl)amino-4′-dicyanovinylbenzene or 2-(2′-hydroxy-5′-methylphenyl)-benzotriazole[37] so that we suggest the scenario in which, at longer pump wavelength, less vibronic excess energy is present in the excited state and hence a small energy barrier associated with $D_1 \rightarrow D_0$ conversion is crossed with a reduced rate. TA-SEC measurements with excitation at 400 nm in the more viscous butyronitrile (*n*BuCN, $\eta = 0.57$ mPa s compared to $\eta = 0.34$ mPa s for MeCN; Figures S27 and S28) were performed. This increase in viscosity lead to a slight increase of τ_1 and τ_2, which were determined to be 11.9 and 36.0 ps, respectively. While the increase of τ_1 and more specifically τ_2 is in line with the model proposed above, the increase is not as substantial as it has been observed, for example, for isomerization reactions. Therefore, further data are likely required for a detailed elucidation of pump-wavelength dependent relaxation in $\mathbf{1}^{\bullet+}$.

In the case of $\mathbf{3}^{\bullet+}$, the general spectral shape and evolution of the signal (Figure S26) is similar to that of $\mathbf{1}^{\bullet+}$. However, the negative differential absorption band becomes more structured for $\mathbf{3}^{\bullet+}$ at later delay times and the decay of the signal is faster, yielding characteristic time constants of <1 and ~15 ps. The shorter time constant describes a concomitant decrease of the GSB as well as the ESA bands and, thus, reveals that the decay pathway to the ground state is more efficient for $\mathbf{3}^{\bullet+}$. The faster relaxation compared to $\mathbf{1}^{\bullet+}$ is ascribed to changes of the excited-state geometry due to the amino group on the phenyl

substituent. This might lead to less structural reorganization in the excited state so that the reorganization energy required during the relaxation process is smaller leading to a faster decay. This hypothesis is based on the fact that the electron-donating properties of the N-substituent of phenothiazines affect the relaxed geometry of the phenyl substituent.[39] A different set of the excited molecules seems to undergo another excited-state relaxation pathway, more specifically one which is accompanied by hole transfer to the aniline substituent. This process leads to a signal growing in at 430 to 490 nm which overlays with the GSB and is attributed to the *N*,*N*-diisobutyl aniline cation radical.[40] After hole transfer to the aromatic substituent takes place, it can formally be treated like an aniline derivative. Due to geometrical restrictions, fast back transfer and decay to the ground state proceed with a characteristic time of around 15 ps. Hole transfer to the substituent is less pronounced upon 800 nm excitation suggesting that the process involves higher lying excited states.

For $\mathbf{2}^{\bullet+}$, the transient absorption signals at early delay times are dominated by two GSB regions at 375 nm and 650 nm as well as an ESA at 410 nm (Figure 7). The latter shifts hypsochromically, similarly to the 540 nm band in the other compounds, and all of the bands decay on a sub-picosecond timescale. The second process is linked to further reduction of the GSB and the build-up of a signal between 410 and 520 nm. The resulting time constants are similar to the ones found for $\mathbf{3}^{\bullet+}$ which, in combination with the spectral changes, suggests that the same processes take place. However, the signal has not completely decayed after 1.8 ns meaning that an additional state is populated in $\mathbf{2}^{\bullet+}$ which does not exist in $\mathbf{3}^{\bullet+}$. This state is characterized by the absorption band between 400 and 520 nm which coincides with the absorption of the *N*,*N*-dimethylaniline cation. With the charge being localized on the substituent, the phenothiazine core is expected to change from a planar geometry, adapted by the radical species, to a bent geometry known for the neutral form.[24b,39b–c] This structural change is supported by DFT calculations (Figure S29) and will concomitantly change the angle between the phenyl ring and the phenothiazine core and reduce the electronic coupling between the two molecular fragments.[37,41] As suggested for other phenothiazine derivatives, this structural reorganization is expected to slow down back transfer which explains the long lifetime of the species $\mathbf{2}^{\bullet+}$ compared to the other two catalysts.[35] This process is most likely not possible for $\mathbf{3}^{\bullet+}$ as a consequence of rotational restriction and steric hindrance due to the methyl groups, which results in lower yields for the photocatalytic products **5** and **6**.

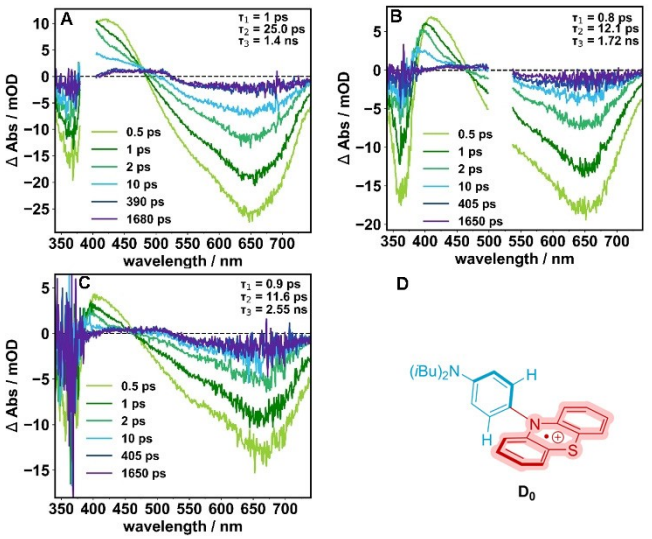

Figure 7. Transient absorption spectra at selected delay times for electrochemically generated $\mathbf{2}^{\bullet+}$ in MeCN pumped at A) 400, B) 528 and C) 800 nm. D) Structure of $\mathbf{2}^{\bullet+}$ in the ground state (D_0). For the DAS, see Figure S25.

Fine-tuning of the photoredox catalytic mechanism

The findings from time-resolved spectroscopy have important implications for the catalytic performance that was observed especially with photocatalyst **2** and give evidence for a photocatalysis based on the absorption of two photons. The second excitation of the radical cation $\mathbf{2}^{\bullet+}$ gives enough driving force to transfer the positive charge from the phenothiazine core to the phenyl substituent that extends the lifetime of this radical cation $\mathbf{2}^{\bullet+}$ overall into the nanosecond range (Figure 8). This was not observed with the photocatalysts **1** and **3**, and both showed lower yields for the photocatalytic borylation and phosphonylation of chlorobenzene (**4**). It is therefore reasonable to assume, firstly, that the long-lived state of $\mathbf{2}^{\bullet+}$ allows for better back electron transfer from the phenyl radical to the catalyst as it gives the reaction partners – bis(pinacolato)diborone or triethyl phosphite – more time to interact. Secondly, back electron transfer to the aniline-like part of the radical cation $\mathbf{2}^{\bullet+}$, where the hole is situated after the second excitation, might be faster and more efficient because of its higher oxidation potential as well as geometric reasons. Compared to the determined oxidation potential of **2**, $E_{ox}(\mathbf{2}^{\bullet+}/\mathbf{2}) = 0.45$ V, which can be assigned to the oxidation of the

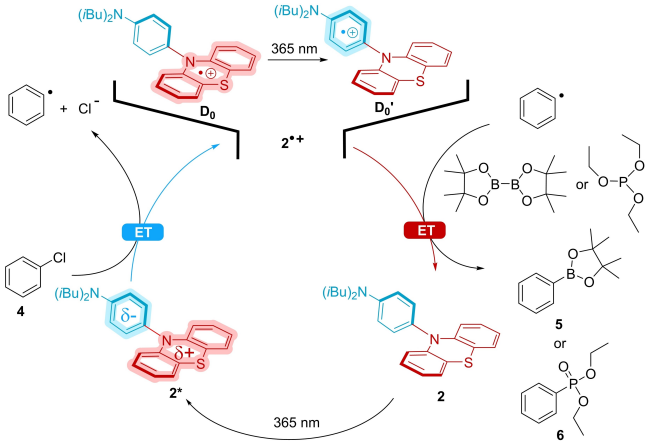

Figure 8. Fine-tuned two-photon photocatalytic cycle for **2**. The second excitation of the radical cation $\mathbf{2}^{\bullet+}$ shifts the positive charge from the phenothiazine core (red) to the phenyl substituent (blue) that extends the overall lifetime of the radical cation $\mathbf{2}^{\bullet+}$ into the ns range and thus facilitates the back electron transfer for more efficient product formation.

phenothiazine core, alkylated anilines have a significantly higher oxidation potential in the range of $E_{ox}(PhNMe_2^{\bullet+}/PhNMe_2) = 0.73–0.84$ V (for *N*,*N*-dimethylaniline).[42] Taken together, this mechanistic scenario explains the higher yields of products observed with photocatalyst **2**. Furthermore, the time-resolved spectra of the radical cation $\mathbf{2}^{\bullet+}$ indicate that two photons and the excited state of both **2** and $\mathbf{2}^{\bullet+}$ are involved in the photoredox catalytic cycle. The mechanism is not a conventional two-photon process with the typical dependence on the light intensity, but similar to the conPET process.[9] In contrast to the conPET concept, however, this photocatalytic cycle does not require a sacrificial electron donor or acceptor as additive to yield the radical ion intermediate state of the photocatalyst.

Substrate scope

With the knowledge of the photoinduced dynamics of the phenothiazine **2**, the scope of the two already mentioned photocatalytic reactions was extended to include a variety of substrates with different electronic structure. The substrate scope of the photoredox catalytic borylation allows a broad variation of the substituents. All photocatalytic experiments were done as triplicates and average yields were reported. Yields of >80% were obtained for the conversion of six of the ten selected substrates (Figure 9), in particular for products **7**–**9** with electron withdrawing groups, such as cyano, fluoro and ester groups. Although also an electron-deficient aromatic molecule, the trifluoromethyl-substituted product **10** was obtained in a moderate yield of 28%. This is probably due to the known hydrolytic sensitivity of the trifluoromethyl group.[43] The twofold borylation starting from 1,4-dichlorobenzene gave product **11** in 56% yield. This product exhibits two functional group tolerances: On the one hand, the presence of the second chloro substituent is tolerated in the first borylation, and, on the other hand, the introduced boronic ester does not interfere in the second borylation. The electron density in *p*-chlorotoluene is slightly increased compared to chlorobenzene rendering the reduction potential more negative to −2.84 V, close to the excited state oxidation potential of photocatalyst **2**. As a result, the yield decreases only slightly, and product **12** can be obtained in a good yield of 71%. For *o*-chloroanisole, the difference in electron density is larger, the reduction potential is shifted to −2.90 V, and product **13** could be obtained in a lower yield of 29%. The conversion of *p*-chloroaniline was not successful, which led to the assumption that the free amino group interferes with the photocatalytic reaction. After protection of the amino group by the *tert*-butylcarbonyl (Boc) group, the substrate could be quantitatively borylated to product **14**. The Boc-protected chloro derivative of the amino acid phenylalanine could also be converted to product **15** in quantitative yield. This is an important result for peptide chemistry.

The mechanism for the borylations is proposed as follows: After excitation of the photocatalyst **2**, it reduces the substrate **4** by single electron transfer. The phenyl radical formed after the release of the chloride anion reacts with the diborone-carbonate adduct previously formed by coordination of

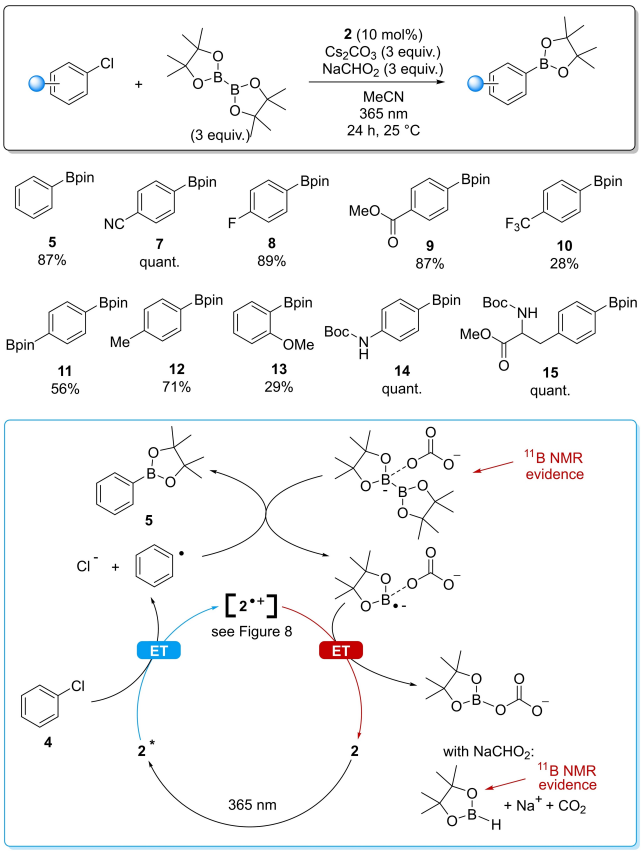

Figure 9. Substrate scope and proposed mechanism for borylations representatively shown for substrate **4**: 0.2 mM substrate in 1 mL total volume (0.2 M), 10 mol% **2**, MeCN, 0.6 mM bis(pinacolato)diborone, 0.6 mM Cs_2CO_3, 0.6 mM $NaCHO_2$, 24 h, 365 nm LED.

carbonate to bis(pinacolato)diborane. This adduct was identified by ^{11}B NMR spectroscopy (Figure S13). After the release of a boronic ester, the remaining boronic acid ester radical anion undergoes protonation and back electron transfer to the catalyst. The latter processes become more efficient with sodium formate as an additive which undergoes an HAT with the borane intermediate. The hydrolyzed borane by-product was detected by ^{11}B NMR spectroscopy (Figure S12). Various control reactions were also carried out to support the proposed mechanism. When sodium formate was omitted, the yield decreased to 54%. This shows that sodium formate is not essential in our photoredox catalytic mechanism which is an advantage compared to the literature examples where stochiometric amounts of sodium formate were required.[44] This can be explained by the mechanistic details derived from the time-resolved measurements: The photoinduced intramolecular hole transfer in the radical cation $\mathbf{2}^{\bullet+}$ extends its overall lifetime and promotes efficient back electron transfer which makes sodium formate not essential. In contrast to sodium formate, the carbonate plays a crucial role in the reaction by activating the bis(pinacolato)diborone.[45] When caesium carbonate was omitted as base, no product was detected at all.

As an alternative to borylations, the phenyl radical can also be trapped by phosphites. The photocatalytic Arbuzov reactions

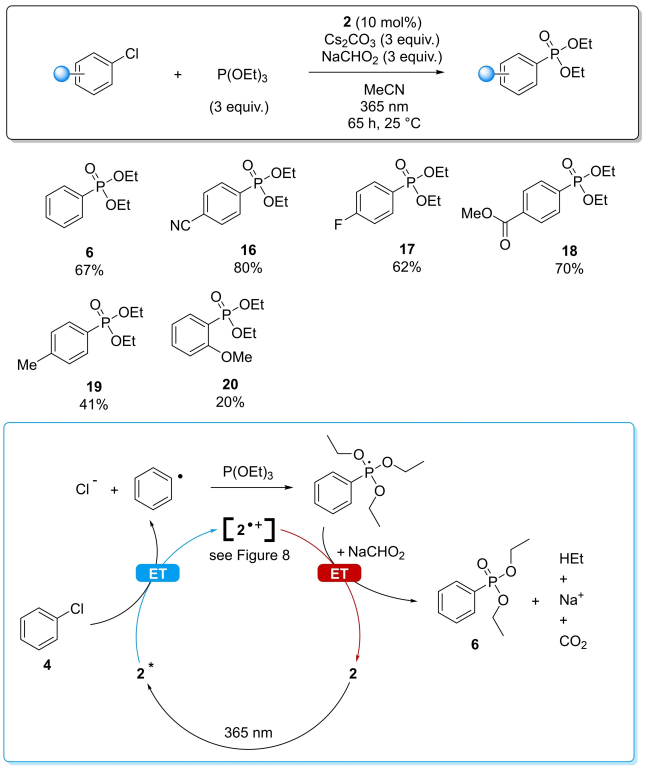

Figure 10. Substrate scope and proposed mechanism for phosphonylations representatively shown for substrate **4**: 0.2 mM substrate in 1 mL total volume (0.2 M), 10 mol% **2**, MeCN, 0.6 mM triethylphosphites, 0.6 mM Cs_2CO_3, 0.6 mM $NaCHO_2$, 24 h, 365 nm LED.

proceeded with lower yields compared to the previously discussed photoredox catalytic borylation, as a countermeasure, the exposure time for the reaction was therefore increased to 65 h (Figure 10).

The substrates with electron-withdrawing substituents are well converted to the products **16**–**18**. Electron-donating groups reduce the yield of products **19** and **20**, as described above for the borylations. The mechanistic proposal includes that the phenyl radical formed after the reduction of chlorobenzene (**4**) by the photocatalyst **2** is captured by triethyl phosphite. This intermediate can subsequently release an ethyl radical, which after the back electron transfer yields the desired diethyl phenyl phosphonate **6**.[46] On the other hand, the release of an ethoxy radical is also possible, leading to the formation of diethyl phenyl phosphonites, which were observed as by-products in the GC-MS analysis. Here again, sodium formate as an additive HAT reagent is not crucial, but the back electron/proton transfer works more efficiently with sodium formate.

Conclusions

Electron-rich phenothiazines are able to activate aryl chlorides to highly reactive aryl radicals simply by photoreduction, which is the initial step for arylations. No additional electrochemical activation setups or any other advanced photocatalysis techniques are needed. This approach can be applied to photocatalytic borylations and Arbuzov reactions using aryl chlorides as starting materials. Due to the extremely strong reduction potential of the dialkylamino substituted phenothiazine **2** in the excited singlet state, $E_{ox}(\mathbf{2}^{\bullet+}/\mathbf{2}^{*}) = -2.9$ V, aryl chlorides with both electron-withdrawing and electron-donating substituents can be activated by photoinduced electron transfer. This activation step is less efficient with the phenyl substituted phenothiazine **1** due to the lower potential of only $E_{ox}(\mathbf{1}^{\bullet+}/\mathbf{1}^{*}) = -2.5$ V. Interestingly, the new photocatalyst **3** with methyl groups in the *ortho* position, unexpectedly, gave lower product yields in the photocatalytic conversions, even though the excited-state potential is sufficiently high ($E_{ox}(\mathbf{3}^{\bullet+}/\mathbf{3}^{*}) = -3.0$ V) and a longer lifetime of a charge-separated state was expected. Time-resolved transient absorption spectroscopy was used to investigate the photophysical properties of the three structurally similar *N*-phenyl phenothiazines. In particular, the cation radicals of photocatalysts **1**–**3** were characterized by means of steady-state and time-resolved spectro-electrochemical methods. This elucidated a second excitation of the radical cation $\mathbf{2}^{\bullet+}$ initiating the transfer of the positive charge onto the phenyl substituent that extends the overall excited-state lifetime of this radical cation into the nanosecond range. Such results were not observed with photocatalysts **1** and **3**; this explains why both the photocatalytic borylations and phosphonylations show higher product yields with **2**. These considerations also suggest that the excited-states of the radicals are involved in the reaction, meaning that a sequential two-photon process takes place. We assume, that the long-lived state of $\mathbf{2}^{\bullet+}$ allows more efficient and faster back electron transfer, because the hole is situated on the aniline part of **2** after the second excitation. Accordingly, sodium formate as additive and HAT reagent are not crucial in these photocatalytic conversions due to the improved photocatalyst, but still induce higher product yields by promoting back electron transfer onto the catalyst. These results show how fine-tuning the radical cation of the chromophore is crucial to improving its performance as an organo-photocatalyst. A detailed and profound understanding of the photophysical properties and the photocatalytic mechanism is essential in advanced photoredox catalysis.

Experimental Section

Materials and methods: All chemicals were purchased from Sigma Aldrich, Fluka, Alfa Aesar, ABCR or Tokyo Chemical industry (TCI). Unless otherwise stated, the chemicals were used as received. Photocatalytic experiments were performed in Fisher Chemical HPLC grade solvents. NMR spectroscopic data were recorded using the following spectrometer hardware: Bruker Avance Neo – ^{1}H NMR (400 MHz), ^{13}C NMR (101 MHz), ^{31}P NMR (162 MHz); Bruker Ascend 500 – ^{1}H NMR (500 MHz), ^{13}C NMR (126 MHz). Chemical shifts of the ^{1}H and ^{13}C NMR spectra are reported in parts per million (ppm) relative to the solvent as an internal standard and was converted to the TMS reference system. Routine ^{13}C NMR spectroscopy was recorded while applying broadband ^{1}H decoupling. Coupling constant (*J*) are given in Hertz (Hz) and the multiplicity of signals are reported as followed: brs (broad singlet), s (singlet), d (doublet), t (triplet), q (quartet), m (multiplet). High-resolution mass spectroscopy was performed using an electron impact ionization source on a Q Exactive Plus Orbitrap from Thermo Scientific. GC analyses were

recorded by using an Agilent 8860 GC instrument using a HP-5 column (30 m×0.32 mm×0.25 μm) and a flame ionization detector (FID). The oven temperature program was: initial temperature 95 °C, hold for 1 min, ramp at 15 °C min^{-1} to 200 °C, hold for 4 min, ramp at 15 °C min^{-1} to 300 °C, hold for 2 min. The injector transfer line temperature was set to 220 °C. Measurements were performed in split-split mode (split ratio 20:1) using Nitrogen as the carrier gas (flow rate 40.0 mL min^{-1}). GC/MS coupling was recorded by using a Varan 431 GC using a capillary FactorFourTM VF-5 ms (30 m×0.25 mm×0.25 μm) and a Varian 210 ion trap mass detector. The oven temperature program was: initial temperature 95 °C, hold for 1 min, ramp at 15 °C min^{-1} to 200 °C, hold for 2 min, ramp at 15 °C min^{-1} to 325 °C, hold for 5 min. The injector transfer line temperature was set to 250 °C. Measurements were performed in split-split mode (split ratio 50:1) using helium as the carrier gas (flow rate 1.0 mL min^{-1}). Thin layer chromatography was performed using Fluka silica gel 60 F_{254} coated aluminum foil. Flash chromatography was performed on silica gel 60, which was prepared by Sigma Aldrich (43–60 μm).

Irradiation of the photochemical reaction was carried out using a setup which was designed and manufactured by the University of Regensburg and the workshop of the Institute for Physical Chemistry at KIT. LEDs of the following types were used to irradiate the samples: Nichia NVSU233A LED. The photoreactions were irradiated from the bottom. The temperature during the reaction time was controlled by using a LAUDA Alpha R8 thermostat. Schlenk tubes, which were provided with either the typical Schlenk stopcock or a Young stopcock, served as reaction vessels.

Synthesis of 1–3: Compounds **1** and **2** were synthesized in one and two steps, respectively, according to the literature.[22] Compound **3** was synthesized in two steps from 3,5-dimethyl aniline over *N,N*-diisobutyl-3,5-dimethylaniline and 4-bromo-*N,N*-diisobutyl-3,5-dimethylaniline.

***N,N*-Diisobutyl-3,5-dimethylaniline**:[48] 1.50 mL of 3,5-dimethylaniline (1.45 g, 12.0 mmol, 1.00 equiv.) was dissolved in 24 mL of EtOH. To this were added 6 mL of H_2O, 1.53 g of Na_2CO_3 (14.4 mmol, 1.20 equiv.), and 3.11 mL of *i*BuBr (3.95 g, 28.8 mmol, 2.40 equiv.), and the mixture was heated to 80 °C for 24 h. The mixture was allowed to cool to RT. Most of the EtOH was removed under reduced pressure and 60 mL of H_2O was added. The mixture was extracted three times with CH_2Cl_2. The combined organic phases were dried over $MgSO_4$. After the solvent was removed under reduced pressure, the crude product was purified by column chromatography (hexane, silica, R_f = 0.81 (hexane/CH_2Cl_2 2:1)). The product was obtained as a yellow solid in a yield of 548 mg (2.35 mmol, 20 %).[48] ^{1}H NMR (400 MHz, $CDCl_3$): δ = 6.31 (s, 1H), 6.29 (s, 2H), 3.13 (d, J = 7.2 Hz, 4H), 2.28 (s, 6H), 2.17–2.02 (m, 2H), 0.91 ppm (d, J = 6.7 Hz, 12H). ^{13}C NMR (101 MHz, $CDCl_3$): δ = 148.56, 138.59, 117.41, 110.53, 60.61, 26.54, 22.07, 20.60 ppm. 2D NMR ($CDCl_3$): COSY, HSQC. HR-ESI-MS: *m/z* (calc.) = 233.2144 [M^+]; *m/z* (found) = 234.2214 [MH^+].

4-Bromo-*N*,*N*-diisobutyl-3,5-dimethylaniline:[49] 574 mg *N,N*-diisobutyl-3,5-dimethylaniline (2.46 mmol, 1.00 equiv.) was dissolved in 11.5 mL CH_2Cl_2 and cooled to −20 °C. Under cooling, a solution of 438 mg NBS (2.46 mmol, 1.00 equiv.) in 15 mL CH_2Cl_2 was slowly added. The reaction mixture was stirred for 30 min at −20 °C. The mixture was then added to 100 mL of brine and extracted three times with 100 mL of Et_2O. The combined organic phases were washed with H_2O and dried over $MgSO_4$. The solvent was removed under reduced pressure and the liquid residue was stored overnight in the freezer. The product was obtained as a pale yellow solid in a yield of 736 mg (2.37 mmol, 96 %).[49] ^{1}H NMR (400 MHz, $CDCl_3$): δ = 6.41 (s, 2H), 3.12 (d, J = 7.3 Hz, 4H,), 2.38 (s, 6H), 2.16–2.00 (m, 2H), 0.91 ppm (d, J = 6.7 Hz, 12H). ^{13}C NMR (101 MHz, $CDCl_3$): δ = 147.00, 138.32, 113.01, 112.71, 60.48, 26.47, 24.54, 20.52 ppm. 2D NMR ($CDCl_3$): COSY, HSQC. HR-ESI-MS: *m/z* (calc.) = 311.1249 [M^+]; *m/z* (found) = 312.1318 [MH^+].

Compound 3: In a heated headspace crimp vial, 129 mg phenothiazine (0.64 mmol, 1.00 equiv.), 301 mg 4-bromo-*N,N*-diisobutyl-3,5 dimethylaniline (0.97 mmol, 1.50 equiv.), 30 mg $Pd_2(dba)_3$ (0.03 mmol, 0.05 equiv.), 155 mg NaOtBu (1.61 mmol, 2.50 equiv.) and 20 mg tricyclohexylphosphine (0.045 mmol, 0.07 equiv.) were placed under argon atmosphere. 3.2 mL of dry toluene was added, and the solution was heated to 120 °C for 65 h. The solution was then allowed to cool to RT. The solvent was removed under reduced pressure and the crude product was purified by column chromatography (hexane/CH_2Cl_2 20:1, silica, R_f = 0.33 (hexane/CH_2Cl_2 2:1)). The product was obtained as a white solid in a yield of 70 mg (0.16 mmol, 25 %). ^{1}H NMR (400 MHz, $CDCl_3$): δ = 6.85 (d, J = 7.4 Hz, 2H), 6.77 (t, J = 7.7 Hz, 2H.), 6.68 (t, J = 7.4 Hz, 2H), 6.45 (s, 2H), 5.99 (d, J = 8.2 Hz, 2H), 3.17 (d, J = 7.1 Hz, 4H), 2.19–2.14 (m, 2H), 2.12 (s, 6H), 0.95 ppm (d, J = 6.6 Hz, 12H).^{13}C NMR (101 MHz, $CDCl_3$): δ = 148.01, 142.36, 138.40, 127.26, 126.25, 125.64, 121.80, 118.39, 114.42, 112.76, 60.56, 26.63, 20.66, 18.73 ppm. 2D NMR ($CDCl_3$): COSY, HSQC. HR-ESI-MS: *m/z* (calc.) = 430.2443 [M^+]; *m/z* (found) = 430.2433 [M^+].

Synthesis of substrates and products: Most of the substrates are commercially available, the syntheses of those that had to be provided are described in the Supporting Information. The products of the photoredox catalytic borylation reactions **5** and **7**–**14** are published.[11,50,51] The others are described in the Supporting Information.

General procedure photoredox catalytic borylation reactions: The corresponding photoredox catalyst, sodium formate, cesium carbonate, the corresponding aryl chloride (if solid) and bis(pinacolato)diboron were placed in a heated Schlenk tube under argon atmosphere. Dry acetonitrile and the corresponding aryl chloride (if liquid) were pipetted in countercurrent with argon. The reaction mixture was degassed four times using the freeze-pump-thaw method. The degassed reaction mixture was stirred at 25 °C and irradiated with light of a wavelength of 365 nm for 24 h. Saturated ammonium chloride solution was then added and the mixture was extracted three times with ethyl acetate. The combined organic phases were dried over magnesium sulfate and the solvent removed under reduced pressure. The residue was taken up in 600 μL deuterated chloroform and transferred into an NMR tube for analysis together with10.0 μL of CH_2Cl_2 (HPLC-grade) as an internal standard. With a density of 1.33 g mL^{-1}, 10.0 μL of CH_2Cl_2 corresponds to 156 μmol. A ^{1}H NMR spectrum was recorded and the integral ratio of the signals from the internal standard and an isolated characteristic product signal was determined. For each sample, the amount of product was calculated using the integral ratio and related to the total batch size. All yields given are mean values of at least three catalytic batches carried out.

General procedure photoredox catalytic phosphorylation reactions (Photo-Arbusov reactions): The corresponding photoredox catalyst, sodium formate and cesium carbonate were placed in a heated Schlenk tube under an argon atmosphere. Dry acetonitrile, triethyl phosphite and the corresponding aryl chloride were pipetted in countercurrent with argon. The reaction mixture was degassed four times using the freeze-pump-thaw method. The degassed reaction mixture was stirred at 25 °C and irradiated with light with a wavelength of 365 nm for 65 h. Appropriate aliquots were then taken for gas chromatographic analysis (see the Supporting Information for a more detailed description).

Sample preparation for spectroscopic experiments: All spectroscopic experiments, that is, steady-state absorption spectro-electro-

chemistry (UV/Vis SEC), and femtosecond time-resolved transient absorption (TA, TASEC) measurements were performed at room temperature. The phenothiazines were dissolved in acetonitrile (Fisher Chemical, $\geq$99.9%, HPLC gradient grade) which has been dried over CaH_2 and degassed prior to use. For measurements in butyronitrile (Thermo Scientific, $\geq$99%) the solvent was used without further purification.

UV/Vis SEC instrumentation: UV/Vis SEC was performed using a three-electrode thin-layer spectro-electrochemical cell with a pathlength of 2 mm (AdValue Technology, USA). The three-electrode system consists of a Pt counter electrode, an Ag/AgCl pseudo-reference electrode and a glassy carbon working electrode. Cyclic voltammetry and chronoamperometric measurements were performed using a computer-controlled VersaSTAT 3 (Princeton Applied Research) potentiostat. UV/Vis spectra were recorded immediately after applying the respective oxidation potential to monitor the accompanied spectral changes. UV/Vis spectra were collected in transmission mode by using a product of Avantes Inc., which is comprised of a single-channel fiber-optic spectrometer (AvaSpec-ULS2048XL) equipped with a deuterium/halogen light source (AvaLight DH-S-BAL). Sample solutions with acetonitrile containing 0.1 M tetrabutylammonium hexafluorophosphate ($TBAPF_6$) as electrolyte were prepared.

Transient absorption spectroscopy:[52–55] A custom-built setup was utilized to acquire fs-TA data. The setup is described in detail elsewhere[1]. The output of an amplified Ti:sapphire laser (Libra, Coherent Inc.), with a pulse-to-pulse repetition rate of 1 kHz and pulses spectrally centered at 800 nm, was split into two beams. One beam is focused into a CaF_2 plate mounted on a rotating stage to generate the white light supercontinuum used as probe pulse. The white light is further split into probe and reference pulse. The probe pulse is focused onto the sample by a concave mirror of 500 mm focal length. The probe pulses are recollimated and spectrally dispersed by a prism and detected by a diode array (Pascher Instruments AB, Sweden). The pump pulses at 400 nm were obtained by second harmonic generation in a BBO crystal whereas for pump pulses centered around 800 nm the output of the Ti:sapphire laser was directly used. The pulses centered around 528 nm were generated by pumping a nonlinear optical-parametric amplifier (TOPAS, Light Conversion). A mechanical chopper reduces the repetition rate of the pump pulses to 0.5 kHz and the polarization is adjusted to the magic angle of 54.7° by a Berek compensator and a polarizer. The spectra were corrected for chirp by fitting a polynomial to the appearance of the maximal signal amplitude at pulse overlap which corresponds to the arrival time of the different wavelengths of the probe pulse. The corresponding time values are then subtracted from the experimental delay time values. The corrected data are globally fitted by a sum of exponentials (parallel model) where the amplitudes of the exponential fit correspond to the decay associated spectra (DAS). During the fitting, the pulse overlap region of $\pm$300 fs was excluded to avoid contributions from coherent artifacts.[54,55] Both, the chirp correction as well as the fit of the data were performed using the KiMoPack software[2] (https://doi.org/10.1021/acs.jpca.2c00907). For the TA-SEC measurements, a quartz cuvette with a pathlength of 1 mm and a three-electrode setup, as described above, were used. The pump and probe beam are directed through a 1-mm hole in the 0.5 mm thick glassy carbon working electrode and spatially overlapped in the sample. Customized electronics and control software (Pascher Instruments AB, Sweden) allow for simultaneously measuring steady state absorption, current, CV, and TA and ensure jitter-free timing of the datasets. Transient absorption spectra of the electrochemically oxidized phenothiazines were recorded at set potentials and constant current response. Steady-state UV/Vis spectra were simultaneously monitored during TA-SEC in order to assess the concentration of the reduced species within the observation volume. All sample solutions were thoroughly degassed with argon prior to each measurement.

Supporting Information

The authors have cited additional references within the Supporting Information.[56–62]

Acknowledgements

Financial support by the Deutsche Forschungsgemeinschaft (DFG, grant Wa 1386/23-1 and DI 1517/23-1) and the Karlsruhe Institute of Technology is gratefully acknowledged. Open Access funding enabled and organized by Projekt DEAL.

Conflict of Interests

The authors declare no conflict of interest.

Data Availability Statement

The data that support the findings of this study are available in the supplementary material of this article.

Keywords: photochemistry · transient absorption spectro-electrochemistry · electrochemistry · borylation · phosphonylation

[1] A. R. Allen, E. A. Noten, C. R. J. Stephenson, *Chem. Rev.* **2022**, *122*, 2695–2751.
[2] a) Q. Liu, C. Huo, Y. Fu, Z. Du, *Org. Biomol. Chem.* **2022**, *20*, 6721–6740; b) T. Bortolato, S. Cuadros, G. Simionato, L. Dell'Amico, *Chem. Commun.* **2022**, *58*, 1263–1283; c) N. A. Romero, D. A. Nicewicz, *Chem. Rev.* **2016**, *116*, 10075–10166; d) T. Bortolato, G. Simionato, M. Vayer, C. Rosso, L. Paoloni, E. M. A. Sartorel, D. Lebœf, L. Dell'Amico, *J. Am. Chem. Soc.* **2023**, *145*, 1835–1846; e) S. Wu, F. Schiel, P. Melchiorre, *Angew. Chem. Int. Ed.* **2023**, *135*, e202306364.
[3] D. P. Hari, B. König, *Angew. Chem. Int. Ed.* **2013**, *52*, 4734–4743.
[4] M. Tobisu, T. Furukawa, N. Chatani, *Chem. Lett.* **2013**, *42*, 1203–1205.
[5] N. Holmberg-Douglas, D. A. Nicewicz, *Chem. Rev.* **2022**, *122*, 1925–2016.
[6] G.-B. Deng, Z.-Q. Wang, J.-D. Xia, P.-C. Qian, R.-J. Song, M. Hu, L.-B. Gong, J.-H. Li, *Angew. Chem. Int. Ed.* **2013**, *52*, 1535–1538.
[7] L. Candish, M. Freitag, T. Gensch, F. Glorius, *Chem. Sci.* **2017**, *8*, 3618–3622.
[8] F. Sandfort, F. Strieth-Kalthoff, F. J. R. Klauck, M. J. James, F. Glorius, *Chem. Eur. J.* **2018**, *24*, 17210–17214.
[9] I. Ghosh, T. Ghosh, J. I. Bardagi, B. König, *Science* **2014**, *346*, 725–728.
[10] I. Ghosh, R. S. Shaikh, B. König, *Angew. Chem. Int. Ed.* **2017**, *56*, 8544–8549.
[11] J. Xu, J. Cao, X. Wu, H. Wang, X. Yang, X. Tang, R. W. Toh, R. Zhou, E. K. L. Yeow, J. Wu, *J. Am. Chem. Soc.* **2021**, *143*, 13266–13273.
[12] I. A. MacKenzie, L. Wang, N. P. R. Onuska, O. F. Williams, K. Begam, A. M. Moran, B. D. Dunietz, D. A. Nicewicz, *Nature* **2020**, *580*, 76–82.
[13] N. G. W. Cowper, C. P. Chernowsky, O. P. Williams, Z. K. Wickens, *J. Am. Chem. Soc.* **2020**, *142*, 2093–2099.
[14] L. Qian, M. Shi, *Chem. Commun.* **2023**, *59*, 3487–3506.

[15] H. Kim, H. Kim, T. H. Lambert, S. Lin, *J. Am. Chem. Soc.* **2020**, *142*, 2087–2092.
[16] N. J. Treat, H. Sprafke, J. W. Kamer, P. G. Clark, B. E. Barton, J. R. d Alaniz, B. P. Fors, C. J. Hawker, *J. Am. Chem. Soc.* **2014**, *136*, 16096–16101.
[17] E. H. Discekici, N. J. Treat, S. O. Poelma, K. M. Mattson, Z. M. Hudson, Y. Luo, C. J. Hawker, J. Read de Alaniz, *Chem. Commun.* **2015**, *51*, 11705–11708.
[18] S. Jin, H. T. Dang, G. C. Haug, R. He, V. D. Nguyen, V. T. Nguyen, H. D. Arman, K. S. Schanze, O. V. Larionov, *J. Am. Chem. Soc.* **2020**, *142*, 1603–1613.
[19] P. Li, A. M. Deetz, J. Hu, G. Meyer, K. Hu, *J. Am. Chem. Soc.* **2022**, *144*, 17604–17610.
[20] Y. Du, R. M. Pearson, C.-H. Lim, S. M. Sartor, M. D. Ryan, H. Yang, N. H. Damrauer, G. M. Miyake, *Chem. Eur. J.* **2017**, *23*, 10962–10968.
[21] a) N. Noto, S. Saito, *ACS Catal.* **2022**, *12*, 15400–15415; b) Y. Li, Z. Ye, Y.-M. Lin, Y. Liu, Y. Zhang, L. Gong, *Nat. Commun.* **2021**, *12*, 2894; c) R. Matsubara, T. Yabuta, U. M. Idros, M. Hayashi, F. Ema, Y. K. K. Sakata, *J. Org. Chem.* **2018**, *83*, 9381–9390; d) N. Toriumi, K. Yamashita, N. Iwasawa, *Chem. Eur. J.* **2021**, *27*, 12635–12641.
[22] F. Speck, D. Rombach, H.-A. Wagenknecht, *Beilstein J. Org. Chem.* **2019**, *15*, 52–59.
[23] a) F. Seyfert, H.-A. Wagenknecht, *Synlett* **2021**, *32*, 582–586; b) F. Weick, D. Steuernagel, A. Belov, H.-A. Wagenknecht, *Synlett* **2022**, *33*, 1199–1203.
[24] a) D. Rombach, H.-A. Wagenknecht, *Angew. Chem. Int. Ed.* **2020**, *59*, 300–303; b) J. Zhou, L. Mao, M.-X. Wu, Z. Peng, Y. Yang, M. Zhou, X.-L. Zhao, X. Shi, H.-B. Yang, *Chem. Sci.* **2022**, *13*, 5252–5260.
[25] a) R. S. Ruoff, K. M. Kadish, P. Boulas, E. C. M. Chen, *J. Phys. Chem.* **1995**, *99*, 8843–8850; b) F. Seyfert, M. Mitha, H.-A. Wagenknecht, *Eur. J. Org. Chem.* **2021**, *2021*, 773–776.
[26] K. A. Margrey, D. A. Nicewicz, *Acc. Chem. Res.* **2016**, *49*, 1997–2006.
[27] N. Miyaura, A. Suzuki, *Chem. Rev.* **1995**, *95*, 2457–2483.
[28] a) A. Michaelis, R. Kaehne, *Chem. Ber.* **1898**, *31*, 1048–1055; b) A. E. Arbusov, *J. Russ. Phys. Chem.* **1906**, *38*, 687.
[29] a) L. Horner, H. Hoffmann, H. G. Wippel, *Chem. Ber.* **1958**, *91*, 64–67; b) L. Horner, H. Hoffmann, H. G. Wippel, G. Klahre, *Chem. Ber.* **1959**, *92*, 2499–2505; c) W. S. Wadsworth, W. D. Emmons, *J. Am. Chem. Soc.* **1961**, *83*, 1733–1738; d) W. S. Wadsworth, W. D. Emmons, *Org. Synth.* **1965**, *45*, 44.
[30] a) M. A. J. Kendall, C. A. Salazar, P. F. Martino, D. R. Tyler, *Organometallics* **2014**, *33*, 6171–6178; b) Z. Zuo, R. S. Kim, D. A. Watson, *J. Am. Chem. Soc.* **2021**, *143*, 1328–1333.
[31] H. N. Ghosh, A. V. Sapre, D. K. Palit, J. P. Mittal, *J. Phys. Chem. B* **1997**, *101*, 2315–2320.
[32] A. C. B. Rodrigues, J. Pina, J. S. S. de Melo, *J. Mol. Liq.* **2020**, *317*, 113966–113987.
[33] J. Daub, R. Engl, J. Kurzawa, S. E. Miller, S. Schneider, A. Stockmann, M. R. Wasielewski, *J. Phys. Chem. A* **2001**, *105*, 5655–5665.
[34] a) S. Jockusch, Y. Yagci, *Polym. Chem.* **2016**, *7*, 6039–6043; b) P. Borowicz, J. Herbich, A. Kapturkiewicz, R. Anulewicz-Ostrowska, J. Nowacki, G. Grampp, *Phys. Chem. Chem. Phys.* **2000**, *2*, 4275–4280.
[35] J. A. Christensen, B. T. Phelan, S. Chaudhuri, A. Acharya, V. S. Batista, M. R. Wasielewski, *J. Am. Chem. Soc.* **2018**, *140*, 5290–5299.
[36] a) S. Jockusch, Y. Yagci, *Polym. Chem.* **2016**, *7*, 6039–6043; b) A. P. Kaur, O. C. Harris, N. H. Attanayake, Z. Liang, S. R. Parkin, M. H. Tang, S. A. Odom, *Chem. Mater.* **2020**, *32*, 3007–3017.
[37] D. Clarke, B. C. Gilbert, P. Hanson, *J. Chem. Soc. Perkin Trans. 2* **1976**, 114–124.
[38] E. Ishow, R. Guillot, G. Buntinx, O. Poizat, *J. Photochem. Photobiol. A* **2012**, *234*, 27–36.
[39] a) D. Clarke, B. C. Gilbert, P. Hanson, C. M. Kirk, *J. Chem. Soc. Perkin Trans. 2* **1978**, 1103–1110; b) T. J. J. M. L. Mayer, *Eur. J. Org. Chem.* **2021**, 3516–3527; c) D. Sun, S. V. Rosokha, J. K. Kochi, *J. Am. Chem. Soc.* **2004**, *126*, 11388–11401.
[40] K. R. G. S. Sumalekshmy, *Chem. Phys. Lett.* **2005**, *413*, 294–299.
[41] M. V. Jovanovic, E. R. Biehl, P. De Meester, S. S. C. Chu, *J. Heterocycl. Chem.* **1984**, *21*, 1425–1429.
[42] a) P. R. Jones, M. J. Drews, J. K. Johnson, P. S. Wong, *J. Am. Chem. Soc.* **2000**, *94*, 4595–4599; b) G. W. Dombrowski, J. P. Dinnocenzo, *J. Org. Chem.* **2005**, *70*, 3791–3800; c) I. Saito, T. Matsuura, K. Inoue, *J. Am. Chem. Soc.* **1983**, *105*, 3200–3206; d) K. Fujimori, T. Takata, S. Fujiwara, O. Kikuchi, S. Oae, *Tetrahedron Lett.* **1986**, *27*, 1617–1620.
[43] a) D. Rombach, H.-A. Wagenknecht, *ChemCatChem* **2018**, *10*, 2955–2961; b) A. Kethe, A. F. Tracy, D. A. Klumpp, *Org. Biomol. Chem.* **2011**, *9*, 4545–4549.
[44] A. J. Boyington, C. P. Seath, A. M. Zearfoss, Z. Xu, N. T. Jui, *J. Am. Chem. Soc.* **2019**, *141*, 4147–4153.
[45] a) S. Wang, H. Wang, B. König, *Chem.* **2021**, *7*, 1653–1665; b) D. Lai, S. Ghosh, A. Hajra, *Org. Biomol. Chem.* **2021**, *19*, 4397–4428.
[46] R. S. Shaikh, S. J. S. Düsel, B. König, *ACS Catal.* **2016**, *6*, 8410–8414.
[47] C. Hansch, A. Leo, R. W. Taft, *Chem. Rev.* **1991**, *91*, 165–195.
[48] T. A. Lutz, P. Spanner, K. T. Wanner, *Tetrahedron* **2016**, *72*, 1579–1589.
[49] D. Wang, M. R. Talipov, M. V. Ivanov, R. Rathore, *J. Am. Chem. Soc.* **2016**, *138*, 16337–16344.
[50] A. F. Chmiel, O. P. Williams, C. P. Chernowsky, C. S. Yeung, Z. A. Wickens, *J. Am. Chem. Soc.* **2021**, *143*, 10882–10889.
[51] A. Nitelet, D. Thevenet, B. Schiavi, C. Hardouin, J. Fournier, R. Tamion, X. Pannecouke, P. Jubault, T. Poisson, *Chem. Eur. J.* **2019**, *25*, 3262–3266.
[52] R. Siebert, D. Akimov, M. Schmitt, A. Winters, U. S. Schubert, B. Dietzek, *ChemPhysChem* **2009**, *10*, 910–919.
[53] C. Müller, T. Pascher, A. Eriksson, P. Chabera, J. Uhlig, *J. Phys. Lett.* **2022**, *126*, 4087–4099.
[54] B. Dietzek, T. Pascher, V. Sundström, A. Yartsev, *Laser Phys. Lett.* **2006**, *4*, 38–43.
[55] A. L. Dobryakova, S. A. Kovalenko, N. P. Ernsting, *J. Chem. Phys.* **2005**, *123*, 44502.
[56] T. Hirao, T. Masunaga, Y. Ohshiro, T. Agawa, *Synthesis* **1981**, *1*, 56–57.
[57] A. J. Moreno-Ortega, F. J. Martínez-Sanz, R. Lajarín-Cuesta, C. de los Rios, M. F. Cano-Abad, *Neuropharmacology* **2015**, *95*, 503–510.
[58] C. Adamo, V. Barone, *J. Chem. Phys.* **1999**, *110*, 6158–6170.
[59] a) F. Weigend, R. Ahlrichs, *Phys. Chem. Chem. Phys.* **2005**, *7*, 3297–3305; b) F. Weigend, *Phys. Chem. Chem. Phys.* **2006**, *8*, 1057–1065.
[60] S. Grimme, S. Ehrlich, L. Goerigk, *J. Comput. Chem.* **2011**, *32*, 1456–1465.
[61] M. J. Frisch, G. W. Trucks, H. B. Schlegel, G. E. Scuseria, M. A. Robb, J. R. Cheeseman, G. Scalmani, V. Barone, G. A. Petersson, H. Nakatsuji, X. Li, M. Caricato, A. V. Marenich, J. Bloino, B. G. Janesko, R. Gomperts, B. Mennucci, H. P. Hratchian, J. V. Ortiz, A. F. Izmaylov, J. L. Sonnenberg, Williams, F. Ding, F. Lipparini, F. Egidi, J. Goings, B. Peng, A. Petrone, T. Henderson, D. Ranasinghe, V. G. Zakrzewski, J. Gao, N. Rega, G. Zheng, W. Liang, M. Hada, M. Ehara, K. Toyota, R. Fukuda, J. Hasegawa, M. Ishida, T. Nakajima, Y. Honda, O. Kitao, H. Nakai, T. Vreven, K. Throssell, J. A. Montgomery Jr., J. E. Peralta, F. Ogliaro, M. J. Bearpark, J. J. Heyd, E. N. Brothers, K. N. Kudin, V. N. Staroverov, T. A. Keith, R. Kobayashi, J. Normand, K. Raghavachari, A. P. Rendell, J. C. Burant, S. S. Iyengar, J. Tomasi, M. Cossi, J. M. Millam, M. Klene, C. Adamo, R. Cammi, J. W. Ochterski, R. L. Martin, K. Morokuma, O. Farkas, J. B. Foresman, D. J. Fox, *Gaussian 16 Rev. C.01*, Wallingford, CT, USA, **2016**.
[62] R. Dennington, T. Keith, J. Millam, *GaussView Ver. 6.1.1*, Shawnee Mission, KS, USA, **2019**.

Manuscript received: July 24, 2023
Accepted manuscript online: August 17, 2023
Version of record online: October 11, 2023